ARTICLES
https://doi.org/10.1038/s41561-019-0326-6
nature geoscience

Craters, boulders and regolith of (101955) Bennu indicative of an old and dynamic surface

K. J. Walsh[1*], E. R. Jawin[2], R.-L. Ballouz[3], O. S. Barnouin[4], E. B. Bierhaus[5], H. C. Connolly Jr.[6], J. L. Molaro[7], T. J. McCoy[2], M. Delbo'[8], C. M. Hartzell[9], M. Pajola[10], S. R. Schwartz[3], D. Trang[11], E. Asphaug[3], K. J. Becker[3], C. B. Beddingfield[12], C. A. Bennett[3], W. F. Bottke[1], K. N. Burke[3], B. C. Clark[13], M. G. Daly[14], D. N. DellaGiustina[3], J. P. Dworkin[15], C. M. Elder[16], D. R. Golish[3], A. R. Hildebrand[17], R. Malhotra[3], J. Marshall[12], P. Michel[8], M. C. Nolan[3], M. E. Perry[4], B. Rizk[3], A. Ryan[8], S. A. Sandford[18], D. J. Scheeres[19], H. C. M. Susorney[20], F. Thuillet[8], D. S. Lauretta[3] and The OSIRIS-REx Team[21]

Small, kilometre-sized near-Earth asteroids are expected to have young and frequently refreshed surfaces for two reasons: collisional disruptions are frequent in the main asteroid belt where they originate, and thermal or tidal processes act on them once they become near-Earth asteroids. Here we present early measurements of numerous large candidate impact craters on near-Earth asteroid (101955) Bennu by the OSIRIS-REx (Origins, Spectral Interpretation, Resource Identification, and Security-Regolith Explorer) mission, which indicate a surface that is between 100 million and 1 billion years old, predating Bennu's expected duration as a near-Earth asteroid. We also observe many fractured boulders, the morphology of which suggests an influence of impact or thermal processes over a considerable amount of time since the boulders were exposed at the surface. However, the surface also shows signs of more recent mass movement: clusters of boulders at topographic lows, a deficiency of small craters and infill of large craters. The oldest features likely record events from Bennu's time in the main asteroid belt.

NASA's OSIRIS-REx (Origins, Spectral Interpretation, Resource Identification, and Security-Regolith Explorer) asteroid sample return mission arrived at near-Earth asteroid (NEA) (101955) Bennu on 3 December 2018. An imaging campaign during the Approach phase of the mission collected panchromatic images with the OSIRIS-REx Camera Suite (OCAMS) PolyCam imager[1–3]. Images collected by the OCAMS MapCam imager[1] during the Preliminary Survey phase of the mission were combined with approach-phase imaging to produce a three-dimensional shape model of the asteroid, revealing a spheroidal spinning-top shape with a diameter of 492 ± 20 m (ref. [4]), as predicted by radar observations[5].

Over the past three decades, ground-based and spacecraft observations of asteroids, combined with theoretical and computational advances, have transformed our understanding of small NEAs (diameters $<\sim$10 km). Observations of NEA shapes, spins and sizes combined with theoretical analyses that have provided insight into their interior properties suggest that NEAs with diameters $>\sim$200 m are 'rubble piles': gravitationally bound, unconsolidated fragments with very low bulk tensile strength[6,7].

Rubble-pile asteroids originate from the main asteroid belt, where catastrophic collisions between larger objects create a population of gravitationally reaccumulated remnants[8]. Small asteroids have limited collisional lifetimes in the main belt ($\sim$0.1 to 1 billion years), and their residence time in the main belt can be shorter than the age of the Solar System due to Yarkovsky drift-induced ejection[9]. After departing the main belt, NEAs are subject to further evolutionary processes, such as rotational spin-up due to thermal torques or tidal effects caused by close planetary flybys[7]. These processes can alter their global and surface morphologies. Studies of the rubble-pile NEA (25143) Itokawa found large boulders exposed on its surface, seemingly rapid degradation of impact craters and evidence of substantial movement of surface material[10]. This suggests that Itokawa has undergone dynamical events[10–12] that operate on timescales shorter than its expected residence time in near-Earth space ($\sim$10 million years)[7].

Detailed study of Bennu's surface geology, particularly the abundance of its craters and morphology of its boulders, provides constraints on the surface age, which is important to disentangle evolutionary processes that operated in near-Earth space from those that operated in the main belt.

Rubble-pile nature of Bennu

The measured density of 1,190 kg m^{-3} and inferred high bulk porosity of Bennu[4,13] and the lack of either high surface slopes or

[1]Southwest Research Institute, Boulder, CO, USA. [2]Smithsonian Institution National Museum of Natural History, Washington, DC, USA. [3]Lunar and Planetary Laboratory, University of Arizona, Tucson, AZ, USA. [4]The Johns Hopkins University Applied Physics Laboratory, Laurel, MD, USA. [5]Lockheed Martin Space, Littleton, CO, USA. [6]Department of Geology, Rowan University, Glassboro, NJ, USA. [7]Planetary Science Institute, Tucson, AZ, USA. [8]Université Côte d'Azur, Observatoire de la Côte d'Azur, CNRS, Laboratoire Lagrange, Nice, France. [9]Department of Aerospace Engineering, University of Maryland, College Park, MD, USA. [10]INAF–Osservatorio Astronomico di Padova, Padova, Italy. [11]Hawai'i Institute of Geophysics and Planetology, University of Hawai'i at Mānoa, Honolulu, HI, USA. [12]SETI Institute, Mountain View, CA, USA. [13]Space Science Institute, Boulder, CO, USA. [14]The Centre for Research in Earth and Space Science, York University, Toronto, Ontario, Canada. [15]NASA Goddard Space Flight Center, Greenbelt, MD, USA. [16]Jet Propulsion Laboratory, California Institute of Technology, Pasadena, CA, USA. [17]Department of Geoscience, University of Calgary, Calgary, AB, Canada. [18]NASA Ames Research Center, Moffett Field, CA, USA. [19]Smead Department of Aerospace Engineering, University of Colorado, Boulder, CO, USA. [20]Department of Earth, Ocean and Atmospheric Sciences, University of British Columbia, Vancouver, British Columbia, Canada. [21]A list of participants and their affiliations appears in the online version of the paper. *e-mail: kwalsh@boulder.swri.edu

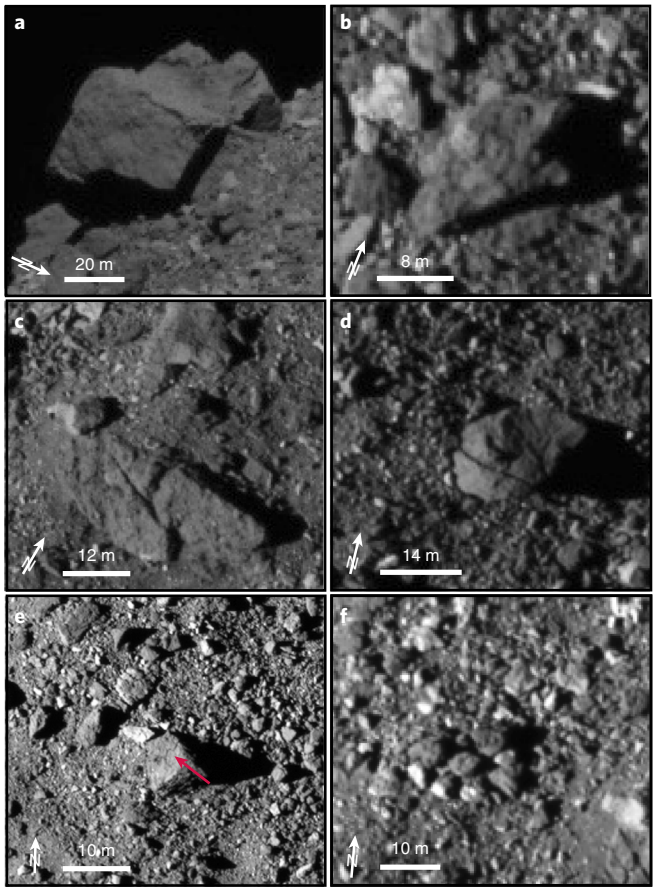

Fig. 1 | The boulders of Bennu can be large and are sometimes fractured or brecciated. a, A boulder located at 48° S and 125° E with a diameter of approximately 56 m and height of over 20 m relative to the surrounding surface of Bennu. **b**, A brecciated boulder located at 6° S and 247° E that is approximately 21 m in diameter with large constituent pieces showing measurable geometric albedo differences[1]. **c**, A boulder with a diameter of approximately 40 m located at 42° N and 129° E that shows a complex web of large fractures. **d**, A boulder with a diameter of approximately 20 m located at 11° S and 258° E with a single linear fracture. **e**, A boulder with a diameter of approximately 10 m located at 5° N and 310° E with a nonlinear fracture (red arrow). **f**, A cluster of metre-sized boulders centred at 44° N and 111° E. Images taken on: **a**, 1 December 2018 from a spacecraft distance of 31.5 km; **b**,**d**, 2 December 2018 from a distance of 24.0 km; **c**, 2 December 2018 from a distance of 23.8 km; **e**, 2 December 2018 from a distance of 24.2 km; **f**, 2 December 2018 from a distance of 23.6 km.

substantial topographic relief indicate that Bennu is a rubble pile. Bennu's density requires 25–50% macroporosity if it is constructed primarily of CI (bulk density of 1,570 kg m^{-3}) or CM (bulk density of 2,200 kg m^{-3}) chondrite-like material[14]. If the microporosity present in these meteorite classes is also considered[15], the total porosity of Bennu may be as high as 60%. In addition, the slope at each point on the surface of Bennu—determined from the combination of the shape, mass and spin state—shows a relaxed distribution with values averaging approximately 17°, and almost entirely below typical angles of approximately 30° allowed by the angle of repose of terrestrial materials and found on other similarly sized NEAs[13,16].

Boulders dominate the local topography of Bennu, some with heights >20 m (Fig. 1a). The most prominent boulder on Bennu was first detected with ground-based radar and estimated to be 10 to 20 m in diameter[2]. This same boulder is apparent in PolyCam images and measures approximately 56 m in its longest dimension (Fig. 1a). There are three identified boulders with long axes exceeding 40 m and more than 200 boulders larger than 10 m[2]. Boulders in the tens-of-metres size range are larger than plausible ejecta from any of the large crater candidates on Bennu[17], and also unlikely to be meteorites that Bennu could have accreted in its current orbit, suggesting instead that their origins trace back to the formation of Bennu in the asteroid belt.

Boulders on Bennu have albedo and colour diversity[1], with some showing these differences within distinct metre-sized clasts in an otherwise unfragmented rock. We interpret such assemblages as impact breccias (Fig. 1b). Processes capable of creating breccias spanning tens of metres with metre-sized clasts imply energetic events that far exceed what Bennu can support[18,19].

The possible inherited origin of Bennu's largest boulders supports the idea that rubble piles form as reaccumulated remnants of disruptive collisions of larger asteroids in the main asteroid belt[8]. Furthermore, the existence of breccias suggests that they are a record of the parent body's accretion, that they formed during impact regolith gardening on the surface of that parent body or that they originated during the catastrophic disruption event that formed Bennu. The noted albedo and colour diversity of the boulders, and the distinct metre-scale components visible in some of them, may point to the compositional diversity of Bennu's parent body and/or its catastrophic impactor.

Boulder geology of Bennu

The spatial distribution of boulders on the surface of Bennu is not uniform. We find concentrations of boulders in some local topographic lows[4] (tens-of-metres elevation differences relative to the surrounding terrain), with boulder abundances up to an order of magnitude greater than the global average (Fig. 2). These collections of boulders stand in contrast to topographic lows on Itokawa, which are distinct for their lack of large boulders and collections of small grains[11].

The boulders on Bennu's surface also exhibit diversity in size, geologic context and morphology. To date, boulders >8 m in diameter have been adequately resolved with PolyCam images, for which we have measured a size-frequency distribution best fit with a power-law index of -2.9 ± 0.3 (ref. [2]). Many of these boulders appear to be resting on top of the surface, while some are partially buried, pointing to active burial and/or exhumation processes. Several examples of imbricated boulders have been identified, although these locations are smaller in extent than the imbricated regions observed on Itokawa[11], with no obvious correlation between imbrication and fine-grained deposits. Both rounded and angular boulders are present on the surface, which may suggest a variety of formation mechanisms, compositions and/or boulder evolutionary processes.

We observe fractured boulders exhibiting multiple fracture types. Some of the most dramatic examples include large, linear fractures that appear to split boulders into two or more pieces (Fig. 1c,d). These occur at all resolvable scales and within some of the largest boulders on the surface. In contrast, other boulders exhibit nonlinear fractures that suggest some interaction between the fracture-driving mechanisms and the rock bulk structure (Fig. 1e). We also found examples of discrete, yet tightly clustered metre-scale boulders that appear to have fractured in situ, and remain in clusters with minimal displacement (Fig. 1f). Complex networks of fractures also occur in some boulders (Fig. 1c,d), with many deep fractures crossing each other at various angles, although some are clearly linear. These numerous and morphologically varied fractures may be produced by one or a combination of processes, such as large-scale impact events, micrometeoroid impacts and thermal fatigue. The latter two processes may also be responsible for the shallow fractures and surficial features observed on visibly textured boulders, which indicate exfoliation, near-surface disaggregation or regolith production processes (for example, refs. [20–22]).

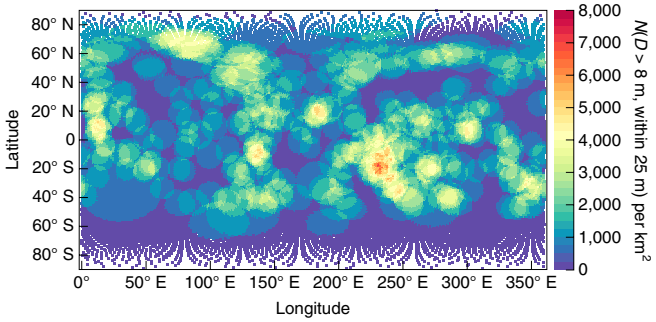

Fig. 2 | Boulder abundance map of the surface of Bennu. The abundance of boulders for each location on the surface of Bennu based on a 49,152-facet shape model of the surface, where the boulder abundance (*N*) is calculated by counting the number of boulders larger than 8 m within a radius of 25 m in each facet and then normalized to square kilometre.

Although boulder fracture could potentially represent past processing on Bennu's parent body, the abundance of fractured boulders and some cases where boulders appear to have disaggregated in situ points to surface processes active in Bennu's recent geologic history, since it evolved to a near-Earth orbit. However, these fracture formation mechanisms need time to operate, suggesting that the surface has not been dynamically refreshed since Bennu's transition from the main belt to its near-Earth orbit, where a typical NEA's dynamical lifetime is on the order of 10 million years[23]. Breakdown due to micrometeoroid bombardment and thermal fatigue is predicted to be faster and slower, respectively, in the main belt than in near-Earth space[20,22,24]. However, the relative efficiencies of these and other active processes are not well constrained, making it difficult to use fractures to assess absolute surface age. Some processes also act over multiple timescales, such as thermal fatigue, which may generate fractures over different spatial scales owing to diurnal and annual thermal cycles.

Craters of Bennu

Bennu has experienced a number of impacts that have transformed its surface. We have identified several tens of candidate impact craters, which range in size from approximately 10 m to more than 150 m in diameter. The characteristics of distinct candidate impact craters include circular features with raised rims and depressed floors, and/or clear textural differences (apparent concentration or lack of boulders) between the interior and exterior of the crater. Less-distinct candidate craters have subdued rims or an absence of raised rims, shallow interiors, and lack of contrast between the interior and exterior boulder populations. Based on current image data, we have identified 12 distinct, and at least 40 less-distinct, candidate craters. Notably, several large distinct craters are located on Bennu's equatorial ridge, suggesting that the ridge is an old feature (Fig. 3).

We used the population of large distinct candidate craters (diameter $D > 50$ m) to estimate the age of Bennu's surface. Assuming that the craters record impact events, they are primarily a record of Bennu's history in the main asteroid belt[25]. Crater scaling laws can convert impact parameters to crater diameters, although for small rubble-pile bodies there is added uncertainty due to their microgravity regime[26,27]. By applying Bennu's physical properties to these scaling relationships (for example, a crater scaling law for dry soil with a strength of 0.18 MPa (ref. [26])), we can estimate the ratio of crater to projectile diameters. The size-frequency distribution of main-belt projectiles striking Bennu is assumed to follow the collisional evolution results[25], while the intrinsic collision probability of Bennu with a main-belt projectile is assumed to be fairly similar to Gaspra, a relatively low inclination asteroid residing in the innermost region of the main belt (where the intrinsic collisional probability is $P_i = 2.8 \times 10^{-18}$ km^{-2} yr^{-1})[28]. These components, when combined with Bennu's cross-section[28], can be fit to Bennu's $D > 50$ m craters. We find that it would take between 100 million and 1 billion years to explain the origin of Bennu's largest crater candidates (Fig. 3d).

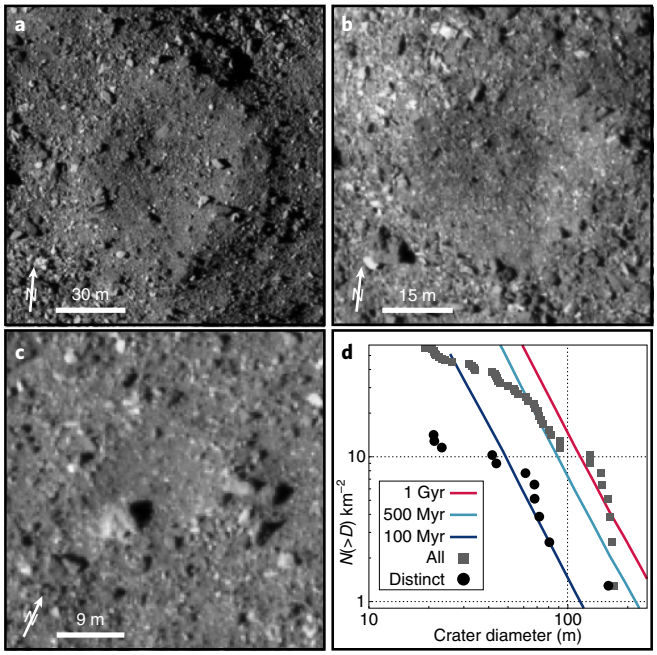

Fig. 3 | Examples of Bennu's craters. a, A feature on Bennu's surface that meets all of the criteria to be considered a distinct candidate crater, including clear topography associated with its rim. This candidate crater is centred at 3° S and 152° E and has a diameter of 81 m. **b**, A distinct candidate crater located at 5° S and 126° E with diameter of 44 m differs in texture between the inside and outside of its rim and shows a distinct lack of boulders. **c**, Example of a less-distinct candidate crater located at 54° N and 68° E, with some textural differences between the inside and outside of the circular feature, but that shows only hints of a circular shape with no clear topography. **d**, The established 'distinct' candidate craters provide a lower bound on age by comparing their distributions to the expected crater production function (see Methods), and we use the entire population of less-distinct candidate craters to estimate an upper bound. In both groups, the change in size-frequency distribution appears around $D = 50$ m. Images taken on: **a**,**b**, 2 December 2018 from a distance of 23.7 km; **c**, 2 December 2018 from a distance of 23.5 km.

However, cratering into low-strength material under low-gravity conditions may lead to larger crater diameters, which in turn could lead to younger age estimates[27]. Conversely, cratering into high-porosity material may lead to reduced diameters and older age estimates[29]. It is possible that determining the surface exposure age of the returned sample will quantitatively constrain Bennu's crater retention age and provide a better understanding of which aspects play dominant roles in crater formation on Bennu and other high-porosity, low-strength targets.

The imaging and topographic data allowed identification of craters approximately 10 m and larger. The observations show a depletion of small craters (~ 10 m $< D < 50$ m) relative to expectations based on the production rate of large craters (Fig. 3d). The depletion of small craters has also been found on other NEAs including Itokawa and Eros[30,31]. The prevalence of boulders on the surface can potentially stifle the formation of small craters, whereby impactors strike and break boulders rather than making craters[32]. Conversely, the depletion of small craters may reflect,

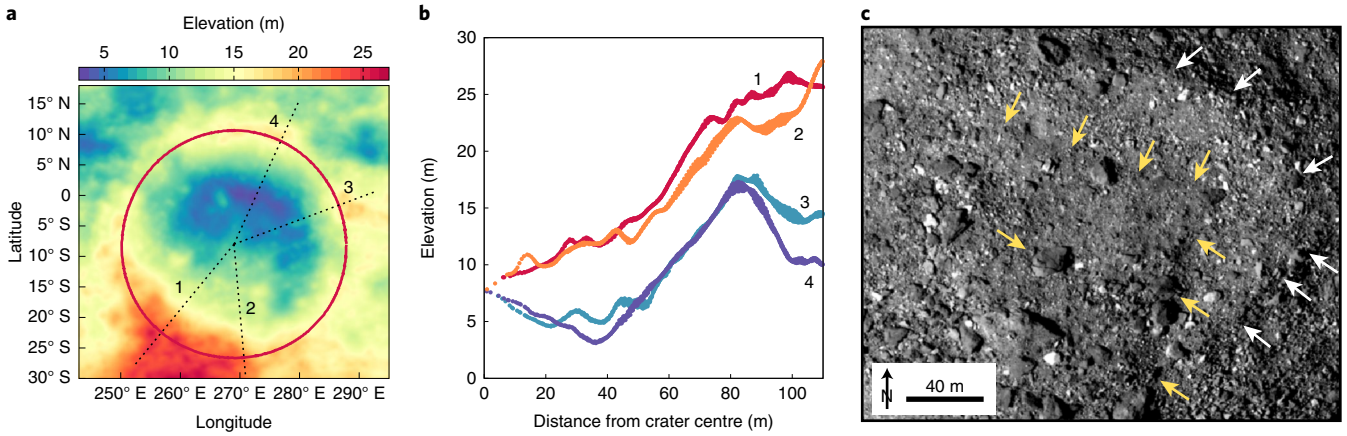

Fig. 4 | Flow of material into a $D = 160$ m candidate crater. a, A large candidate crater is centred near the equator at 8° S and 269° E, and initial measurements indicate a diameter of 160 m. The drawn circle outlines the crater rim and four dotted lines indicate profiles along which elevation was extracted radially from the centre of the crater outward. **b**, The elevation profiles for the different regions of the crater, where the profiles 1 and 2 show that the southwest region of the crater is elevated relative to the rest of the crater shown with profiles 3 and 4. The mass movement appears to have overtopped the crater rim and covered parts of the crater with metres of material. **c**, Image showing the relationship between the material flow and the candidate crater. White arrows indicate the crater rim, and yellow arrows indicate the edge of the flow which has entered the crater from the west (the flow correlates with the elevated portion of topographic profiles 1 and 2). Stratigraphic relationships show that the flow occurred after the formation of the crater. Leftmost yellow arrow indicates additional material movement that has partly buried the westernmost portion of a larger boulder (which is also shown in Fig. 1c). Image used for **c** was taken on 1 December 2018 from a distance of 31.8 km.

as previously postulated, crater erasure due to surface material movement and/or seismic shaking[33,34]. There are clear examples on some large candidate craters on Bennu of material movement and crater infill, where the thickness of the fill layer is comparable to the depth of small craters (Fig. 4)[4].

Regolith of Bennu

The interiors of many small candidate impact craters ($D < 20$ m) are largely devoid of resolvable boulders (Fig. 3). These locations may be reservoirs for smaller particles produced or exposed during the crater formation process. Similarly, boulder-fracturing processes or abrasion and mechanical erosion between boulders during surface material movement could each contribute to the production of fine grains more widely across the surface of Bennu.

There is some evidence that fine-grained material (of the centimetre-scale sizes that are ingestible by the OSIRIS-REx sample mechanism[35] and of smaller, micrometre-scale sizes) is present despite not being resolved with current imaging. The measured thermal inertia is consistent with a population of centimetre-sized particles[2]. The phase reddening observed with the MapCam images suggest some photometric contribution by micrometre-sized particles[2]. Thermal emission spectra[14] exhibit evidence of a surface dominated by particles greater than 125 µm at spatial scales of approximately 80 m, but these data cannot provide more specific information on the range of particle sizes greater than 125 µm or rule out the presence of a small fraction of particles smaller than 125 µm.

Finally, certain regions only a few metres in size have large albedo differences and lack observable boulders, suggesting that they are dominated by unresolved (<1 m) particles[1]. Other fine-particulate patches appear as surficial layers indiscriminately draped over boulder and inter-boulder areas alike[2]. However, low-albedo deposits do not mask the outlines of boulders. The dark material comprising these patches may be dust or fine particles.

History of Bennu

The large boulders on the surface of Bennu may provide information about the composition and geology of its parent body, as well as the collision that disrupted it. The observed impact breccias may have formed during the evolution of its parent body, through repeated impact events on its surface over most of Solar System history, or during the large impact event that resulted in the formation of Bennu. Alternatively, these breccias may even date to the accretion of the original parent body in the protoplanetary disk.

The retention of large craters on Bennu's equatorial ridge requires that the surface age predates the expected approximately 10-million-year duration as a NEA. There is no clear geologic indication of the process that formed the ridge, and given its relation to the large craters it could be a feature preserved from the formation of Bennu[36], which would make it the oldest feature on its surface[4,13,31]. Bennu's surface therefore also recorded processes from its time in the main belt; the formation timescales of the largest craters suggest that Bennu recorded hundreds of millions of years of history during this period.

Bennu retains very old craters despite evidence of continued and varied surface evolution. The processes that have removed small craters may be size limited or spatially localized and therefore cannot efficiently erase larger craters. The crater infill observed on the largest distinct crater has deposited an approximately 5-m-thick layer of material inside the crater and has partially degraded a large swath of the crater rim (Fig. 4). If surface material movement of this scale were to act widely and frequently, it could contribute to large-scale resurfacing of the asteroid. However, the old age of the surface of Bennu indicates that this type of event may either be localized, or of low frequency, possibly occurring only during its time as an NEA.

Resurfacing and surface movement will have influenced and resorted the fine-grained surface material that is the final target of the OSIRIS-REx mission[37]. The returned sample of this material will tell us about processes that occurred since Bennu has been a NEA, while Bennu was in the main belt, and likely processes that occurred on its original parent body and in the solar nebula long before Bennu formed.

Online content

Any methods, additional references, Nature Research reporting summaries, source data, statements of data availability and associated accession codes are available at https://doi.org/10.1038/s41561-019-0326-6.

Received: 28 January 2019; Accepted: 11 February 2019;
Published online: 19 March 2019

References

1. Lauretta, D. S. et al. The unexpected surface of asteroid (101955) Bennu. *Nature* https://doi.org/10.1038/s41586-019-1033-6 (2019).
2. DellaGiustina, D. N. et al. Properties of rubble-pile asteroid (101955) Bennu from OSIRIS-REx imaging and thermal analysis. *Nat. Astron.* https://doi.org/10.1038/s41550-019-0731-1 (2019).
3. Rizk, B. et al. OCAMS: the OSIRIS-REx camera suite. *Space Sci. Rev.* **214**, 26 (2018).
4. Barnouin, O. S. et al. Shape of (101955) Bennu indicative of a rubble pile with internal stiffness. *Nat. Geosci.* https://doi.org/10.1038/s41561-019-0330-x (2019).
5. Nolan, M. C. et al. Shape model and surface properties of the OSIRIS-REx target asteroid (101955) Bennu from radar and lightcurve observations. *Icarus* **226**, 629–640 (2013).
6. Richardson, D. C., Leinhardt, Z. M., Melosh, H. J., Bottke, W. F. & Asphaug, E. in *Asteroids III* (eds Bottke, W. F. Jr, Cellino, A., Paolicchi, P. & Binzel, R. P.) 501–515 (Univ. Arizona Press, 2002).
7. Walsh, K. J. Rubble pile asteroids. *Annu. Rev. Astron. Astrophys.* **56**, 593–624 (2018).
8. Michel, P., Benz, W., Tanga, P. & Richardson, D. C. Collisions and gravitational reaccumulation: forming asteroid families and satellites. *Science* **294**, 1696–1700 (2001).
9. Bottke, W. F. et al. Dynamical spreading of asteroid families by the Yarkovsky effect. *Science* **294**, 1693–1696 (2001).
10. Fujiwara, A. et al. The rubble-pile asteroid Itokawa as observed by Hayabusa. *Science* **312**, 1330 (2006).
11. Miyamoto, H. et al. Regolith migration and sorting on asteroid Itokawa. *Science* **316**, 1011–1014 (2007).
12. Hirata, N. et al. A survey of possible impact structures on 25143 Itokawa. *Icarus* **200**, 486 (2009).
13. Scheeres, D. N. et al. The dynamic geophysical environment of (101955) Bennu based on OSIRIS-REx measurements. *Nat. Astron.* https://doi.org/10.1038/s41550-019-0721-3 (2019).
14. Hamilton, V. E. et al. Evidence for widespread hydrated minerals on asteroid (101955) Bennu. *Nat. Astron.* https://doi.org/10.1038/s41550-019-0722-2 (2019).
15. Macke, R. J., Consolmagno, G. J. & Britt, D. T. Density, porosity, and magnetic susceptibility of carbonaceous chondrites. *Meteorit. Planet. Sci.* **46**, 1842–1862 (2011).
16. Ostro, S. J. et al. Radar imaging of binary near-Earth asteroid (66391) 1999 KW4. *Nature* **314**, 1276–1280 (2006).
17. Bart, G. D. & Melosh, H. J. Using lunar boulders to distinguish primary from distant secondary impact craters. *Geophys. Res. Lett.* **34**, L07203 (2007).
18. Bischoff, A., Edward, R. D. S., Metzler, K. & Goodrich, C. A. in *Meteorites and the Early Solar System II* (eds Lauretta, D. S. & McSween H. Y. Jr) 679–712 (Univ. Arizona Press, 2006).
19. Noguchi, T. et al. Surface morphological features of boulders on Asteroid 25143 Itokawa. *Icarus* **206**, 319–326 (2010).
20. Molaro, J. L., Byrne, S. & Le, J. L. Thermally induced stresses in boulders on airless body surfaces, and implications for rock breakdown. *Icarus* **294**, 247–261 (2017).
21. Delbo', M. et al. Thermal fatigue as the origin of regolith on small asteroids. *Nature* **508**, 233–236 (2014).
22. Basilevsky, A. T., Head, J. W., Horz, F. & Ramsley, K. Survival times of meter-sized rock boulders on the surface of airless bodies. *Planet. Space Sci.* **117**, 312–328 (2015).
23. Gladman, B., Michel, P. & Froeschlé, C. The near-Earth object population. *Icarus* **146**, 176–189 (2000).
24. Graves, K. J., Minton, D. A., Molaro, J. L. & Hirabayashi, M. Resurfacing asteroids from thermally induced surface degradation. *Icarus* **322**, 1–12 (2019).
25. Bottke, W. F. et al. The fossilized size distribution of the main asteroid belt. *Icarus* **175**, 111–140 (2005).
26. Holsapple, K. A. The scaling of impact processes in planetary sciences. *Ann. Rev. Earth Planet. Sci.* **21**, 333–373 (1993).
27. Holsapple, K. A. & Housen, K. R. A crater and its ejecta: an interpretation of Deep Impact. *Icarus* **187**, 345–356 (2007).
28. Bottke, W. F., Nolan, M. C., Greenberg, R. & Kolvoord, R. A. Velocity distributions among colliding asteroids. *Icarus* **107**, 255–268 (1994).
29. Prieur, N. C. et al. The effect of target properties on transient crater scaling for simple craters. *J. Geophys. Res. Planets* **122**, 1704–1726 (2017).
30. Thomas, P. C. & Robinson, M. S. Seismic resurfacing by a single impact on the asteroid 433 Eros. *Nature* **436**, 366–369 (2005).
31. Michel, P., O'Brien, D. P., Abe, S. & Hirata, N. Itokawa's cratering record as observed by Hayabusa: implications for its age and collisional history. *Icarus* **200**, 503–513 (2009).
32. Tatsumi, E. & Sugita, S. Cratering efficiency on coarse-grain targets: Implications for the dynamical evolution of asteroid 25143 Itokawa. *Icarus* **300**, 227–248 (2017).
33. Richardson, J. E., Melosh, H. J., Greenberg, R. J. & O'Brien, D. P. The global effects of impact-induced seismic activity on fractured asteroid surface morphology. *Icarus* **179**, 325–349 (2005).
34. Asphaug, E. Critical crater diameter and asteroid impact seismology. *Meteorit. Planet. Sci.* **43**, 1075–1084 (2008).
35. Bierhaus, E. B. et al. The OSIRIS-REx spacecraft and the touch-and-go sample acquisition mechanism (TAGSAM). *Space Sci. Rev.* **214**, 107 (2018).
36. Michel, P. et al. Disruption and reaccumulation as the possible origins of Ryugu and Bennu top shapes. In *Lunar Planetary Sci. Conf. 50* abstr. 1659 (2019).
37. Lauretta, D. S. et al. OSIRIS-REx: sample return from asteroid (101955) Bennu. *Space Sci. Rev.* **212**, 925–984 (2017).

Acknowledgements

This material is based on work supported by NASA under contracts NNM10AA11C and NNH09ZDA007O issued through the New Frontiers Program. M.P. was supported for this research by the Italian Space Agency (ASI) under the ASI-INAF agreement no. 2017–37-H.0. M.D., P.M., and A.R. would like to acknowledge the French space agency CNES. M.D., A.R., P.M. and S.R.S acknowledge support from the Academies of Excellence on Complex Systems and Space, Environment, Risk and Resilience of the Initiative d'EXcellence 'Joint, Excellent, and Dynamic Initiative' (IDEX JEDI) of the Université Côte d'Azur. Part of this work was performed at the Jet Propulsion Laboratory, California Institute of Technology, under contract with the National Aeronautics and Space Administration.

Author contributions

K.J.W. led the mapping, analysis and manuscript writing. E.R.J., R.-L.B., O.S.B., E.B.B., H.C.C., J.L.M. and T.J.M. contributed to the mapping, analysis and writing of the manuscript. D.S.L. leads the mission and contributed to analysis and writing. M.D., C.M.H., M.P., S.R.S. and D.T. contributed to mapping and manuscript writing. E.A., K.J.B., C.B.B., W.F.B., C.A.B., K.N.B., B.C.C., M.G.D., D.N.D., J.P.D., C.M.E., D.R.G., A.R.H., R.M., J.M., P.M., M.C.N., M.E.P., B.R., A.R., D.J.S., H.C.C., S.A.S., H.C.M.S. and F.T. all contributed to the mapping, analysis or manuscript writing. The entire OSIRIS-REx Team made the Bennu encounter possible.

Competing interests

The authors declare no competing interests.

Additional information

Reprints and permissions information is available at www.nature.com/reprints.

Correspondence and requests for materials should be addressed to K.J.W.

Publisher's note: Springer Nature remains neutral with regard to jurisdictional claims in published maps and institutional affiliations.

Methods

Initial boulder identification was carried out following the methods outlined in ref. [2]. Subsequent detailed mapping and geologic analyses of boulders were performed by a visual analysis of PolyCam and MapCam data using the Small Body Mapping Tool (SBMT), which projects spacecraft images onto a shape model[38]. Boulders were mapped by drawing an ellipse around the resolved boulder margins; this method allows for the analysis of both long and intermediate axis lengths, as well as boulder orientation. Boulders were viewed under a range of viewing geometries including various phase angles and illumination angles. Detailed boulder morphology was assessed using a combination of unprojected images which facilitated fine-scale analyses, and projected images within SBMT, which provides geologic context. Boulder abundance (Fig. 2) was calculated using a 49,152-facet shape model[4], where the boulder abundance was calculated by counting the number of boulders larger than 8 m within a 25 m radius in each facet and then normalizing to 1 km^2. Image for Fig. 1a is ocams20181201t055746s307_pol_iofl2pan_63551 taken on 1 December 2018 from a spacecraft distance of 31.5 km. Fig. 1b,d is from image ocams20181202t072303s706_pol_iofl2pan_63785 taken on 2 Decemeber 2018 with a spacecraft distance 24.0 km. Fig. 1c is taken from image ocams20181202t082747s619_pol_iofl2pan_63714 taken on 2 December 2018 with a spacecraft distance of 23.8 km. Fig. 1e is taken from image 20181202T064001S485_pol_iofL2pan taken on 2 December 2018 with a spacecraft distance of 24.2 km. Fig. 1f is taken from image20181202T084918S806_pol_iofL2pan taken on 2 December 2018 with a spacecraft distance of 23.6 km.

Crater identification and measurement was performed using a combination of projected and unprojected PolyCam and MapCam images, as well as stereophotoclinometry-derived topography data[4]. All mapping was carried out in SBMT by mapping ellipses around the maximum extent of the resolvable crater rim. Multiple members of the team mapped the surface for craters and only those mapped by multiple members as distinct crater candidates were counted in the 'distinct' category for the purposes of analysis. All mapped individual craters were included in the 'non-distinct' group. To calculate surface age, we used the largest craters to estimate a range of possible surface ages based on the impactor size distribution found in the main belt, an average main-belt impact probability and impact velocity ($P_i = 2.8 \times 10^{-18}$ km^{-2} yr^{-1} and $v_i = 5.3$ km s^{-1})[25,39], and a crater scaling law for dry soil with a strength of 0.18 MPa (ref. [26]). The clearly established 'distinct' candidate craters, normalized to one square kilometre, provide a lower bound on age, and we use the entire population of less-distinct candidate craters to estimate an upper bound. In both groups, the change in size-frequency distribution appears around $D = 50$ m. Image ocams20181202t083822s735_pol_iofl2pan_64172 was used for Fig. 3a,b and was taken on 2 December 2018 from a spacecraft range of 23.7 km. Image for Fig. 3c was ocams20181202t091159s321_pol_iofl2pan_64104 and was taken on 2 December 2018 from a spacecraft range of 23.5 km. Image ocams20181201t051455s588_pol_iofl2pan_63071 was used for Fig. 4c and was taken on 1 December 2018 from a spacecraft distance of 31.8 km.

Many of the geologic assessments relied on elevation, which was derived from shape model v14. The construction of the shape model, and different versions of the shape model, and calculation of elevation is described in detail in a companion paper[4].

Data availability

Raw through to calibrated datasets will be available via the Planetary Data System (PDS) (https://sbn.psi.edu/pds/resource/orex/). Data are delivered to the PDS according to the OSIRIS-REx Data Management Plan available in the OSIRIS-REx PDS archive. Higher-level products, for example, global mosaics and elevation maps, will be available in the PDS one year after departure from the asteroid.

References

38. Ernst, C. M., Barnouin, O. S. & Daly, R. T. The Small Body Mapping Tool (SBMT) for accessing, visualizing, and analyzing spacecraft data in three dimensions. In *Lunar Planetary Sci. Conf. 49* abstr. 1043 (2018).
39. Marchi et al. The cratering history of (2867) Steins. *Planet. Space Sci.* **58**, 1116–1123 (2010).

The OSIRIS-REx Team

D. E. Highsmith[22], J. Small[22], D. Vokrouhlický[23], N. E. Bowles[24], E. Brown[24], K. L. Donaldson Hanna[24], T. Warren[24], C. Brunet[25], R. A. Chicoine[25], S. Desjardins[25], D. Gaudreau[25], T. Haltigin[25], S. Millington-Veloza[25], A. Rubi[25], J. Aponte[26], N. Gorius[26], A. Lunsford[26], B. Allen[27], J. Grindlay[27], D. Guevel[27], D. Hoak[27], J. Hong[27], D. L. Schrader[28], J. Bayron[29], O. Golubov[30], P. Sánchez[30], J. Stromberg[31], M. Hirabayashi[32], C. M. Hartzell[9], S. Oliver[33], M. Rascon[33], A. Harch[34], J. Joseph[34], S. Squyres[34], D. Richardson[35], J. P. Emery[36], L. McGraw[36], R. Ghent[37], R. P. Binzel[38], M. M. Al Asad[20], C. L. Johnson[7,20], L. Philpott[20], H. C. M. Susorney[20], E. A. Cloutis[39], R. D. Hanna[40], H. C. Connolly Jr.[6], F. Ciceri[17], A. R. Hildebrand[17], E.-M. Ibrahim[17], L. Breitenfeld[41], T. Glotch[41], A. D. Rogers[41], B. E. Clark[42], S. Ferrone[42], C. A. Thomas[43], H. Campins[44], Y. Fernandez[44], W. Chang[45], A. Cheuvront[46], D. Trang[11], S. Tachibana[47], H. Yurimoto[47], J. R. Brucato[48], G. Poggiali[48], M. Pajola[10], E. Dotto[49], E. Mazzotta Epifani[49], M. K. Crombie[50], C. Lantz[51], M. R. M. Izawa[52], J. de Leon[53], J. Licandro[53], J. L. Rizos Garcia[53], S. Clemett[54], K. Thomas-Keprta[54], S. Van wal[55], M. Yoshikawa[55], J. Bellerose[16], S. Bhaskaran[16], C. Boyles[16], S. R. Chesley[16], C. M. Elder[16], D. Farnocchia[16], A. Harbison[16], B. Kennedy[16], A. Knight[16], N. Martinez-Vlasoff[16], N. Mastrodemos[16], T. McElrath[16], W. Owen[16], R. Park[16], B. Rush[16], L. Swanson[16], Y. Takahashi[16], D. Velez[16], K. Yetter[16], C. Thayer[56], C. Adam[57], P. Antreasian[57], J. Bauman[57], C. Bryan[57], B. Carcich[57], M. Corvin[57], J. Geeraert[57], J. Hoffman[57], J. M. Leonard[57], E. Lessac-Chenen[57], A. Levine[57], J. McAdams[57], L. McCarthy[57], D. Nelson[57], B. Page[57], J. Pelgrift[57], E. Sahr[57], K. Stakkestad[57], D. Stanbridge[57], D. Wibben[57], B. Williams[57], K. Williams[57], P. Wolff[57], P. Hayne[58], D. Kubitschek[58], M. A. Barucci[59], J. D. P. Deshapriya[59], S. Fornasier[59], M. Fulchignoni[59], P. Hasselmann[59], F. Merlin[59], A. Praet[59], E. B. Bierhaus[5], O. Billett[5], A. Boggs[5], B. Buck[5], S. Carlson-Kelly[5], J. Cerna[5], K. Chaffin[5], E. Church[5], M. Coltrin[5], J. Daly[5], A. Deguzman[5], R. Dubisher[5], D. Eckart[5], D. Ellis[5], P. Falkenstern[5], A. Fisher[5], M. E. Fisher[5], P. Fleming[5], K. Fortney[5], S. Francis[5], S. Freund[5], S. Gonzales[5], P. Haas[5], A. Hasten[5], D. Hauf[5], A. Hilbert[5], D. Howell[5], F. Jaen[5], N. Jayakody[5], M. Jenkins[5], K. Johnson[5], M. Lefevre[5], H. Ma[5], C. Mario[5], K. Martin[5], C. May[5], M. McGee[5], B. Miller[5], C. Miller[5], G. Miller[5], A. Mirfakhrai[5], E. Muhle[5], C. Norman[5], R. Olds[5], C. Parish[5], M. Ryle[5], M. Schmitzer[5], P. Sherman[5], M. Skeen[5], M. Susak[5], B. Sutter[5], Q. Tran[5], C. Welch[5], R. Witherspoon[5], J. Wood[5], J. Zareski[5], M. Arvizu-Jakubicki[3], E. Asphaug[3], E. Audi[3], R.-L. Ballouz[3], R. Bandrowski[3], K. J. Becker[3], T. L. Becker[3], S. Bendall[3], C. A. Bennett[3], H. Bloomenthal[3], D. Blum[3], W. V. Boynton[3], J. Brodbeck[3], K. N. Burke[3], M. Chojnacki[3], A. Colpo[3], J. Contreras[3], J. Cutts[3], C. Y. Drouet d'Aubigny[3], D. Dean[3], D. N. DellaGiustina[3], B. Diallo[3], D. Drinnon[3], K. Drozd[3], H. L. Enos[3], R. Enos[3], C. Fellows[3], T. Ferro[3], M. R. Fisher[3], G. Fitzgibbon[3], M. Fitzgibbon[3], J. Forelli[3], T. Forrester[3], I. Galinsky[3], R. Garcia[3], A. Gardner[3], D. R. Golish[3], N. Habib[3], D. Hamara[3], D. Hammond[3], K. Hanley[3], K. Harshman[3], C. W. Hergenrother[3], K. Herzog[3], D. Hill[3], C. Hoekenga[3], S. Hooven[3], E. S. Howell[3], E. Huettner[3], A. Janakus[3], J. Jones[3], T. R. Kareta[3], J. Kidd[3], K. Kingsbury[3], S. S. Balram-Knutson[3], L. Koelbel[3], J. Kreiner[3], D. Lambert[3], D. S. Lauretta[3], C. Lewin[3], B. Lovelace[3], M. Loveridge[3], M. Lujan[3], C. K. Maleszewski[3], R. Malhotra[3], K. Marchese[3], E. McDonough[3], N. Mogk[3], V. Morrison[3], E. Morton[3], R. Munoz[3], J. Nelson[3], M. C. Nolan[3], J. Padilla[3], R. Pennington[3], A. Polit[3], N. Ramos[3], V. Reddy[3], M. Riehl[3], B. Rizk[3], H. L. Roper[3], S. Salazar[3], S. R. Schwartz[3], S. Selznick[3], N. Shultz[3], P. H. Smith[3], S. Stewart[3], S. Sutton[3], T. Swindle[3], Y. H. Tang[3], M. Westermann[3], C. W. V. Wolner[3], D. Worden[3], T. Zega[3], Z. Zeszut[3], A. Bjurstrom[60], L. Bloomquist[60], C. Dickinson[60], E. Keates[60], J. Liang[60], V. Nifo[60], A. Taylor[60], F. Teti[60], M. Caplinger[61], H. Bowles[62], S. Carter[62],

S. Dickenshied[62], D. Doerres[62], T. Fisher[62], W. Hagee[62], J. Hill[62], M. Miner[62], D. Noss[62], N. Piacentine[62], M. Smith[62], A. Toland[62], P. Wren[62], M. Bernacki[63], D. Pino Munoz[63], S.-i. Watanabe[55,64], S. A. Sandford[18], A. Aqueche[15], B. Ashman[15], M. Barker[15], A. Bartels[15], K. Berry[15], B. Bos[15], R. Burns[15], A. Calloway[15], R. Carpenter[15], N. Castro[15], R. Cosentino[15], J. Donaldson[15], J. P. Dworkin[15], J. Elsila Cook[15], C. Emr[15], D. Everett[15], D. Fennell[15], K. Fleshman[15], D. Folta[15], D. Gallagher[15], J. Garvin[15], K. Getzandanner[15], D. Glavin[15], S. Hull[15], K. Hyde[15], H. Ido[15], A. Ingegneri[15], N. Jones[15], P. Kaotira[15], L. F. Lim[15], A. Liounis[15], C. Lorentson[15], D. Lorenz[15], J. Lyzhoft[15], E. M. Mazarico[15], R. Mink[15], W. Moore[15], M. Moreau[15], S. Mullen[15], J. Nagy[15], G. Neumann[15], J. Nuth[15], D. Poland[15], D. C. Reuter[15], L. Rhoads[15], S. Rieger[15], D. Rowlands[15], D. Sallitt[15], A. Scroggins[15], G. Shaw[15], A. A. Simon[15], J. Swenson[15], P. Vasudeva[15], M. Wasser[15], R. Zellar[15], J. Grossman[65], G. Johnston[65], M. Morris[65], J. Wendel[65], A. Burton[66], L. P. Keller[66], L. McNamara[66], S. Messenger[66], K. Nakamura-Messenger[66], A. Nguyen[66], K. Righter[66], E. Queen[67], K. Bellamy[68], K. Dill[68], S. Gardner[68], M. Giuntini[68], B. Key[68], J. Kissell[68], D. Patterson[68], D. Vaughan[68], B. Wright[68], R. W. Gaskell[7], L. Le Corre[7], J.-Y. Li[7], J. L. Molaro[7], E. E. Palmer[7], M. A. Siegler[7], P. Tricarico[7], J. R. Weirich[7], X.-D. Zou[7], T. Ireland[69], K. Tait[70], P. Bland[71], S. Anwar[72], N. Bojorquez-Murphy[72], P. R. Christensen[72], C. W. Haberle[72], G. Mehall[72], K. Rios[72], I. Franchi[73], B. Rozitis[73], C. B. Beddingfield[12], J. Marshall[12], D. N. Brack[19], A. S. French[19], J. W. McMahon[19], D. J. Scheeres[19], E. R. Jawin[2], T. J. McCoy[2], S. Russell[3], M. Killgore[74], W. F. Bottke[1], V. E. Hamilton[1], H. H. Kaplan[1], K. J. Walsh[1], J. L. Bandfield[13], B. C. Clark[13], M. Chodas[75], M. Lambert[75], R. A. Masterson[75], M. G. Daly[14], J. Freemantle[14], J. A. Seabrook[14], O. S. Barnouin[4], K. Craft[4], R. T. Daly[4], C. Ernst[4], R. C. Espiritu[4], M. Holdridge[4], M. Jones[4], A. H. Nair[4], L. Nguyen[4], J. Peachey[4], M. E. Perry[4], J. Plescia[4], J. H. Roberts[4], R. Steele[4], R. Turner[18], J. Backer[76], K. Edmundson[76], J. Mapel[76], M. Milazzo[76], S. Sides[76], C. Manzoni[77], B. May[77], M. Delbó[8], G. Libourel[8], P. Michel[8], A. Ryan[8], F. Thuillet[8] and B. Marty[78]

[22]Aerospace Corporation, Chantilly, VA, USA. [23]Astronomical Institute, Charles University, Prague, Czech Republic. [24]Atmospheric, Oceanic and Planetary Physics, University of Oxford, Oxford, UK. [25]Canadian Space Agency, Saint-Hubert, Quebec, Canada. [26]Catholic University of America, Washington, DC, USA. [27]Center for Astrophysics, Harvard University, Cambridge, MA, USA. [28]Center for Meteorite Studies, Arizona State University, Tempe, AZ, USA. [29]City University of New York, New York, NY, USA. [30]Colorado Center for Astrodynamics Research, University of Colorado, Boulder, CO, USA. [31]Commonwealth Scientific and Industrial Research Organisation (CSIRO), Canberra, Australian Capital Territory, Australia. [32]Department of Aerospace Engineering, Auburn University, Auburn, AL, USA. [33]Department of Astronomy and Steward Observatory, University of Arizona, Tuscon, AZ, USA. [34]Department of Astronomy, Cornell University, Ithaca, NY, USA. [35]Department of Astronomy, University of Maryland, College Park, MD, USA. [36]Department of Earth and Planetary Sciences, University of Tennessee, Knoxville, TN, USA. [37]Department of Earth Sciences, University of Toronto, Toronto, Ontario, Canada. [38]Department of Earth, Atmospheric, and Planetary Sciences, Massachusetts Institute of Technology, Cambridge, MA, USA. [39]Department of Geography, University of Winnipeg, Winnipeg, Manitoba, Canada. [40]Department of Geological Sciences, Jackson School of Geosciences, University of Texas, Austin, TX, USA. [41]Department of Geosciences, Stony Brook University, Stony Brook, NY, USA. [42]Department of Physics and Astronomy, Ithaca College, Ithaca, NY, USA. [43]Department of Physics and Astronomy, Northern Arizona University, Flagstaff, AZ, USA. [44]Department of Physics, University of Central Florida, Orlando, FL, USA. [45]Edge Space Systems, Greenbelt, MD, USA. [46]General Dynamics C4 Systems, Denver, CO, USA. [47]Hokkaido University, Sapporo, Japan. [48]INAF–Astrophysical Observatory of Arcetri, Florence, Italy. [49]INAF–Osservatorio Astronomico di Roma, Rome, Italy. [50]Indigo Information Services, Tucson, AZ, USA. [51]Institut d'Astrophysique Spatiale, CNRS/Université Paris Sud, Orsay, France. [52]Institute for Planetary Materials, Okayama University–Misasa, Misasa, Japan. [53]Instituto de Astrofísica de Canarias and Departamento de Astrofísica, Universidad de La Laguna, Tenerife, Spain. [54]Jacobs Technology, Houston, TX, USA. [55]JAXA Institute of Space and Astronautical Science, Sagamihara, Japan. [56]Kavli Institute for Astrophysics and Space Research, Massachusetts Institute of Technology, Cambridge, MA, USA. [57]KinetX Aerospace, Inc., Simi Valley, CA, USA. [58]Laboratory for Atmospheric and Space Physics, University of Colorado, Boulder, CO, USA. [59]LESIA, Observatoire de Paris, Université PSL, CNRS, Sorbonne Université, Univ. Paris Diderot, Sorbonne Paris Cité, Meudon, France. [60]Macdonald, Dettwiler, and Associates, Brampton, Ontario, Canada. [61]Malin Space Science Systems, San Diego, CA, USA. [62]Mars Space Flight Facility, Arizona State University, Tempe, AZ, USA. [63]Mines ParisTech, Paris, France. [64]Nagoya University, Nagoya, Japan. [65]NASA Headquarters, Washington, DC, USA. [66]NASA Johnson Space Center, Houston, TX, USA. [67]NASA Langley Research Center, Hampton, VA, USA. [68]NASA Marshall Space Flight Center, Huntsville, AL, USA. [69]Research School of Earth Sciences, Australian National University, Canberra, Australian Capital Territory, Australia. [70]Royal Ontario Museum, Toronto, Ontario, Canada. [71]School of Earth and Planetary Sciences, Curtin University, Perth, Western Australia, Australia. [72]School of Earth and Space Exploration, Arizona State University, Tempe, AZ, USA. [73]School of Physical Sciences, The Open University, Milton Keynes, UK. [74]Southwest Meteorite Laboratory, Payson, AZ, USA. [75]Space Systems Laboratory, Department of Aeronautics and Astronautics, Massachusetts Institute of Technology, Cambridge, MA, USA. [76]US Geological Survey Astrogeology Science Center, Flagstaff, AZ, USA. [77]London Stereoscopic Company, London, UK. [78]Université de Lorraine, Nancy, France.